

Low-voltage and fast-response polymer-stabilized hyper-twisted nematic liquid crystal

Jiamin Yuan,¹ Guanjun Tan,¹ Daming Xu,¹ Fenglin Peng,¹ Alexander Lorenz,² and Shin-Tson Wu^{1,*}

¹CREOL, The College of Optics and Photonics, University of Central Florida, Orlando, FL 32816, USA

²Stranski-Laboratorium, TU Berlin, Sekretariat TC 9, Str. des 17. Juni 124, 10623 Berlin, Germany

*swu@ucf.edu

Abstract: We report a low-voltage and submillisecond-response polymer-stabilized hyper-twisted-nematic (HTN) liquid crystal cell with a large dielectric anisotropy host mixture. To correct the measured voltage-dependent transmittance, we have to take the voltage shielding effect of the alignment layers into consideration. Both Kerr effect and flexoelectro-optic effect contribute to the observed induced birefringence. To evaluate the dynamic responses of these two effects, we fit the decay time data with a double relaxation model. A good agreement between the experiment and simulation is obtained. Such a HTN cell still exhibits fast response time (<2ms) even at low temperature (0°C). Potential applications for display and photonic devices are foreseeable.

©2015 Optical Society of America

OCIS codes: (160.3710) Liquid crystals; (230.3720) Liquid-crystal devices.

References and links

1. M. Schadt, "Milestone in the history of field-effect liquid crystal displays and materials," *Jpn. J. Appl. Phys.* **48**(3), 03B001 (2009).
2. H. Chen, M. Hu, F. Peng, J. Li, Z. An, and S.-T. Wu, "Ultra-low viscosity liquid crystal materials," *Opt. Mater. Express* **5**(3), 655–660 (2015).
3. S. Gauza, X. Zhu, W. Piecek, R. Dabrowski, and S. T. Wu, "Fast switching liquid crystals for color-sequential LCDs," *J. Disp. Technol.* **3**(3), 250–252 (2007).
4. D. Xu, L. Rao, C. D. Tu, and S. T. Wu, "Nematic liquid crystal display with submillisecond grayscale response time," *J. Disp. Technol.* **9**(2), 67–70 (2013).
5. J. W. Kim, T. H. Choi, and T. H. Yoon, "Fast switching of nematic liquid crystals over a wide temperature range using a vertical bias electric field," *Appl. Opt.* **53**(26), 5856–5859 (2014).
6. D. J. Channin, "Triode optical gate - New liquid-crystal electro-optic device," *Appl. Phys. Lett.* **26**(11), 603–605 (1975).
7. H. Kikuchi, M. Yokota, Y. Hisakado, H. Yang, and T. Kajiyama, "Polymer-stabilized liquid crystal blue phases," *Nat. Mater.* **1**(1), 64–68 (2002).
8. J. S. Patel and R. B. Meyer, "Flexoelectric electro-optics of a cholesteric liquid crystal," *Phys. Rev. Lett.* **58**(15), 1538–1540 (1987).
9. L. Rao, J. Yan, S. T. Wu, S. I. Yamamoto, and Y. Haseba, "A large Kerr constant polymer-stabilized blue phase liquid crystal," *Appl. Phys. Lett.* **98**(8), 081109 (2011).
10. M. Wittek, N. Tanaka, D. Wilkes, M. Bremer, D. Pauluth, J. Canisius, A. Yeh, R. Yan, K. Skjonnemand, and M. Klasen-Memmer, "4.4: New materials for polymer-stabilized blue phase," *SID Int. Symp. Digest Tech. Papers* **43**(1), 25–28 (2012).
11. Y. Haseba, S.-i. Yamamoto, K. Sago, A. Takata, and H. Tobata, "22.1: Invited Paper: Low-voltage polymer-stabilized blue-phase liquid crystals," *SID Int. Symp. Digest Tech. Papers* **44**(1), 254–257 (2013).
12. Y. Chen, D. Xu, S. T. Wu, S. Yamamoto, and Y. Haseba, "A low voltage and submillisecond-response polymer-stabilized blue phase liquid crystal," *Appl. Phys. Lett.* **102**(14), 141116 (2013).
13. L. Rao, H. C. Cheng, and S. T. Wu, "Low voltage blue-phase LCDs with double-penetrating fringe fields," *J. Disp. Technol.* **6**(8), 287–289 (2010).
14. L. Rao, Z. Ge, S. T. Wu, and S. H. Lee, "Low voltage blue-phase liquid crystal displays," *Appl. Phys. Lett.* **95**(23), 231101 (2009).
15. F. Peng, Y. Chen, J. Yuan, H. Chen, S. T. Wu, and Y. Haseba, "Low temperature and high frequency effects on polymer-stabilized blue phase liquid crystals with large dielectric anisotropy," *J. Mater. Chem. C* **2**(18), 3597–3601 (2014).

16. B. J. Broughton, M. J. Clarke, S. M. Morris, A. E. Blatch, and H. J. Coles, "Effect of polymer concentration on stabilized large-tilt-angle flexoelectro-optic switching," *J. Appl. Phys.* **99**(2), 023511 (2006).
17. D. J. Gardiner, S. M. Morris, F. Castles, M. M. Qasim, W. S. Kim, S. S. Choi, H. J. Park, I. J. Chung, and H. J. Coles, "Polymer stabilized chiral nematic liquid crystals for fast switching and high contrast electro-optic devices," *Appl. Phys. Lett.* **98**(26), 263508 (2011).
18. A. Lorenz, D. J. Gardiner, S. M. Morris, F. Castles, M. M. Qasim, S. S. Choi, W. S. Kim, H. J. Coles, and T. D. Wilkinson, "Electrical addressing of polymer stabilized hyper-twisted chiral nematic liquid crystals with interdigitated electrodes: Experiment and model," *Appl. Phys. Lett.* **104**(7), 071102 (2014).
19. H. Coles, S. Morris, F. Castles, D. Gardiner, and Q. Malik, "40.1: Invited Paper: Ultrafast high optical contrast flexoelectric displays for video frame rates," *SID Int. Symp. Digest Tech. Papers* **43**(1), 544–547 (2012).
20. F. Castles, S. M. Morris, and H. J. Coles, "Flexoelectro-optic properties of chiral nematic liquid crystals in the uniform standing helix configuration," *Phys. Rev. E Stat. Nonlin. Soft Matter Phys.* **80**(3), 031709 (2009).
21. M. Jiao, Z. Ge, Q. Song, and S. T. Wu, "Alignment layer effects on thin liquid crystal cells," *Appl. Phys. Lett.* **92**(6), 061102 (2008).
22. J. Yan, H. C. Cheng, S. Gauza, Y. Li, M. Jiao, L. Rao, and S. T. Wu, "Extended Kerr effect of polymer-stabilized blue-phase liquid crystals," *Appl. Phys. Lett.* **96**(7), 071105 (2010).
23. T. Ishitani, Y. Niikura, M. Ikenaga, M. Kobayashi, M. Kato, T. Nagi, Y. Oe, M. Nakano, S. Seo, Y. Hirakata, J. Koyama, S. Yamazaki, R. Sato, K. Okazaki, and M. Katayama, "4.2: Polymer-stabilized blue-phase material driven at low voltage," *SID Int. Symp. Digest Tech. Papers* **43**(1), 18–21 (2012).
24. H. Lee, H.-J. Park, O.-J. Kwon, S. J. Yun, J. H. Park, S. Hong, and S.-T. Shin, "11.1: Invited Paper: The world's first blue phase liquid crystal display," *SID Int. Symp. Digest Tech. Papers* **42**(1), 121–124 (2011).
25. C. Y. Tsai, C. Y. Tsai, F. C. Yu, Y. F. Lan, P. J. Huang, S. Y. Lin, Y. T. Chen, T. I. Tsao, C. T. Hsieh, B. S. Tseng, C. W. Kuo, C. H. Lin, C. C. Kuo, C. H. Chen, H. Y. Hsieh, C. T. Chuang, and N. Sugiura, "A novel blue phase liquid crystal display applying wall-electrode and high driving voltage circuit," *SID Int. Symp. Dig. Tech. Pap.* #37.1 (2015).
26. D. Xu, Y. Chen, Y. Liu, and S. T. Wu, "Refraction effect in an in-plane-switching blue phase liquid crystal cell," *Opt. Express* **21**(21), 24721–24735 (2013).
27. P. R. Gerber, "Electro-optical effects of a small-pitch blue-phase system," *Mol. Cryst. Liq. Cryst. (Phila. Pa.)* **116**(3–4), 197–206 (1985).
28. H. J. Coles, B. Musgrave, M. J. Coles, and J. Willmott, "The effect of the molecular structure on flexoelectric coupling in the chiral nematic phase," *J. Mater. Chem.* **11**(11), 2709–2716 (2001).
29. H. J. Coles, M. J. Clarke, S. M. Morris, B. J. Broughton, and A. E. Blatch, "Strong flexoelectric behavior in bimesogenic liquid crystals," *J. Appl. Phys.* **99**(3), 034104 (2006).
30. C. Noot, M. J. Coles, B. Musgrave, S. P. Perkins, and H. J. Coles, "The flexoelectric behaviour of a hypertwisted chiral nematic liquid crystal," *Mol. Cryst. Liq. Cryst. (Phila. Pa.)* **366**(1), 725–733 (2001).
31. M. Schadt and F. Muller, "Physical-properties of new liquid-crystal mixtures and electrooptical performance in twisted nematic displays," *IEEE Electron. Dev.* **25**(9), 1125–1137 (1978).
32. S. T. Wu, A. M. Lackner, and U. Efron, "Optimal operation temperature of liquid crystal modulators," *Appl. Opt.* **26**(16), 3441–3445 (1987).
33. D. Xu, J. Yan, J. Yuan, F. Peng, Y. Chen, and S. T. Wu, "Electro-optic response of polymer-stabilized blue phase liquid crystals," *Appl. Phys. Lett.* **105**(1), 011119 (2014).

1. Introduction

Fast response time is one of the most critical requirements for liquid crystal display (LCD) and photonic devices [1] because it helps reduce motion picture image blur and crosstalk, enhance optical efficiency, and suppress color mixing for field-sequential displays. Extensive efforts have been devoted to reduce the response time by developing ultra-low viscosity nematic LCs [2] or reducing the cell gap [3], but the fastest response time achieved so far is still around several milliseconds. For color sequential displays, in order to suppress color breakup the required response time should be below one millisecond. Some triode approaches [4, 5] have been proposed to achieve submillisecond response time, but the required driving scheme remains too complicated to be implemented in active matrix LCDs since the first concept reported about four decades ago [6].

Recently, two promising LC modes with submillisecond response time are emerging: polymer-stabilized blue phase liquid crystal (BPLC) [7] and polymer-stabilized hyper-twisted nematic (HTN) liquid crystals [8]. There are some similarities and differences between BPLC and HTN. In terms of similarity, both LCs are optically isotropic in the voltage-off state, provided that Bragg reflection is in the UV region, and they all exhibit fast response time. However, there are three major differences: (1) Physical mechanisms: BPLC is based on Kerr effect, but HTN involves both Kerr effect and flexoelectro-optic effect; (2) Surface alignment:

BPLC is a self-assembly 3D lattice structure so that no surfactant (e.g., polyimide layer) is needed to generate uniform molecular alignment, while HTN requires surface alignment layers; (3) Curing temperature: BPLC precursor has a fairly narrow blue phase temperature range, so that the curing temperature has to be controlled precisely. For HTN, there is no special requirement; it can be cured conveniently at room temperature. For both BPLC and HTN, high operation voltage is their common problem. To reduce the on-state voltage of BPLC, high $\Delta\epsilon$ LC materials [9–12] and protruded electrode structures [13, 14] have been developed. Nevertheless, its electro-optic effect is quite sensitive to the temperature and frequency [15]. For example, at 5°C the response time of BPLC could exceed 10 ms, if the employed LC host has a large $\Delta\epsilon$. For HTN, two types of molecular arrangement have been proposed: uniform lying helix (ULH) [16] and uniform standing helix (USH) [17, 18]. Each configuration has its own pros and cons. For ULH devices, the major challenge is to uniformly align the optical axes of helical structures on the substrate. A non-uniform optical axis distribution leads to low contrast ratio [19]. On the other hand, USH exhibits a high contrast ratio (>3000:1), but its operation voltage is still quite high (>15V/ μm) [17, 18, 20]. Moreover, there is no report that HTN still possesses fast response time at low temperature. There is an urgent need to develop new material and device structure to lower the operation voltage while keeping fast response time at low temperature.

In this paper, we investigated the coupled flexoelectro-optic and Kerr effects of our polymer-stabilized HTN in USH mode. We employed a large $\Delta\epsilon$ nematic LC to enhance the Kerr effect so that the operation voltage can be reduced compared to that of pure flexoelectro-optic devices. Our HTN precursor can be UV cured at room temperature and it does not need precise temperature control. Meanwhile, it exhibits very fast response time (<2 ms) even at 0°C. To understand the underlying physical mechanisms, we developed a numerical model by incorporating the extended Kerr model with flexoelectric effect, and taking into account the voltage shielding effect from alignment layers. Our simulation results agree with experiment well. Also, we investigated the temperature-dependent response time and analyzed the dynamic responses of HTN using a double-relaxation model. The simulation results successfully describe the temperature-dependent relaxation processes of HTN and this provides a useful guideline for future device optimization.

2. Mixture formulation

In experiment, we employed a large $\Delta\epsilon$ nematic LC host HTG-135200 (HCCH, China) whose physical properties are: $\Delta n = 0.205$ at $\lambda = 633$ nm, $\Delta\epsilon = 100.3$ at 1 kHz and 23°C, and clearing temperature $T_c = 96^\circ\text{C}$. The precursor consists of 86.45 wt. % HTG, 4.55 wt. % chiral dopant R5011 (HCCH), 5.4 wt. % RM257 (Merck), 3.6 wt. % TMPTA (1,1,1-Trimethylolpropane Triacrylate, Sigma Aldrich). This material was carefully chosen because it has an appropriate $\Delta\epsilon$ value. If the $\Delta\epsilon$ is too small, then the operation voltage would be too high for practical applications. On the other hand, if the $\Delta\epsilon$ is too large (>300), then several problems would occur, such as huge viscosity and low Debye relaxation frequency [15], which in turn causes the electro-optic effects to be too sensitive to the temperature and frequency. Also, some materials with a large $\Delta\epsilon$ by adding polar groups like cyano would attract ions. As a result, the voltage holding ratio is inadequate. Fortunately, after extensive material development effort some commercial high $\Delta\epsilon$ LC materials have been tested with good stability and reliability in prototype display panels. Here, we chose a delicate material to balance the operation voltage, temperature, and frequency. Note that R5011 is employed due to its high helical twisting power. The resulting pitch length of our polymer-stabilized HTN was measured to be 178nm. The HTN precursor was then filled into an LC cell with in-plane switching (IPS) electrodes and cell gap $d \sim 8.82\mu\text{m}$. The IPS cell consisted of interdigitated pixel electrodes on the bottom substrate (electrode width $w = 15\mu\text{m}$, spacing $l = 15\mu\text{m}$, abbreviated as IPS-15/15). A thin (~ 80 nm) polyimide (PI) alignment layer was over-coated on the inner surface of each substrate. The rubbing angle was perpendicular to the electrode stripes, i.e., parallel to the

electric field. With this rubbing direction, we can achieve the highest transmittance when the rubbing angle is oriented at 45° w.r.t. the polarizer. So this is a typical USH cell. Next, we exposed the cell with UV light ($\lambda \sim 365$ nm, intensity 8 mW/cm²) for 30 min at room temperature. For measurement purpose, the sample was sandwiched between two crossed linear polarizers. A He-Ne laser ($\lambda = 633$ nm) was used as a probing beam. Due to the short pitch length of our material, this material has unnoticeable reflection [20] at $\lambda = 633$ nm, which ensures an optically isotropic dark state at $V = 0$ so that high contrast ratio can be achieved.

3. Material characterization

3.1 VT characteristics

We measured the voltage-dependent transmittance (VT) curve of the HTN IPS-15/15 cell, as shown by the black dotted line in Fig. 1. The cell exhibits a peak transmittance of $\sim 55\%$ at $V = 104V_{\text{rms}}$. Here the transmittance is normalized to two parallel polarizers in order to exclude the absorption loss of polarizers. The relatively low transmittance and high voltage result from the large electrode width and gap of the IPS-15/15 cell. Large electrode width causes a big dead-zone on top of the electrode, resulting in a lower transmittance. On the other hand, large electrode gap demands a higher voltage. A promising solution to overcome these two important issues will be discussed later.

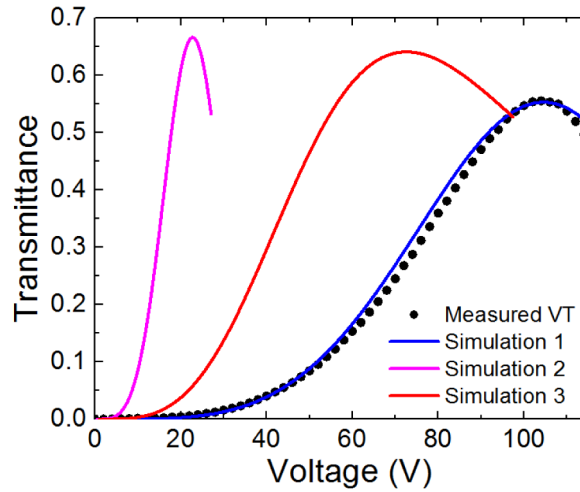


Fig. 1. Measured VT curve of an IPS-15/15 cell (black dotted line) and corresponding simulation (blue solid line); Model of an IPS-2/4 cell with flat electrodes (red solid line) and $3.5\mu\text{m}$ protruded electrodes (pink solid line).

To fit the measured data with theory, we need to first correct the voltage shielding effect from alignment layers. The HTN cell can be treated as three capacitors (two alignment layers and one LC layer) in series, so the effective voltage on the LC layer (V_{LC}) can be derived as [21]:

$$V_{LC} = \frac{V_{AP}}{\left(1 + \frac{2\varepsilon_{LC}d_{AL}}{\varepsilon_{AL}d_{LC}}\right)}, \quad (1)$$

where V_{AP} is the applied voltage, ε_{LC} is the effective dielectric constant of the LC layer at a given voltage, ε_{AL} is the dielectric constant of the alignment layer, and d_{LC} and d_{AL} are the thicknesses of the LC layer and alignment layer, respectively. From Eq. (1), for a LC layer that has very large ε_{LC} as in our experiment, the voltage shielding effect is more serious. In

this case, an alignment layer which has a large ϵ_{AL} and small d_{AL} is preferred. For our cell, $\epsilon_{AL} = 3.4$ so we find $V_{LC} \sim 0.8V_{AP}$.

Lorenz, *et al.* reported a model to characterize the Kerr and flexoelectro-optic effects for polymer-stabilized chiral nematic LCs [18]. In the model, the induced birefringence from Kerr effect is described by $\Delta n_k = \lambda KE^2$. This original Kerr model is valid only in the low field region, because the induced birefringence cannot increase unlimitedly with the electric field. The maximum induced birefringence from Kerr effect should be clamped by the material itself, which can be expressed by an exponential convergence equation known as the extended Kerr model [22]:

$$\Delta n_k = \Delta n_s \cdot \left[1 - \exp\left(-\frac{E}{E_s}\right)^2 \right], \quad (2)$$

where Δn_s stands for the saturated refractive index change and E_s represents the saturation field. Hence, we incorporated Eq. (2) into Lorenz's model and then added this term to the induced birefringence from the flexoelectric effect, which can be described by:

$$\theta_m = \arctan\left(\frac{2e_f p E_x}{2\pi(k_{11} + k_{33})}\right), \quad (3)$$

$$n_{eff} = \sqrt{\frac{n_e^2 + n_o^2}{2}}, \quad (4)$$

$$\Delta n_f = n_{eff} - \left(\left(\frac{\cos(\theta_m)}{n_{eff}} \right)^2 + \left(\frac{\sin(\theta_m)}{n_o} \right)^2 \right)^{-1/2}, \quad (5)$$

where θ_m represents the maximum induced tilt angle by the electric field component E_x (perpendicular to the helical axis); p is the pitch length and e_f is the flexoelectric coefficient. Finally, the total induced birefringence is summed as $\Delta n = \Delta n_k + \Delta n_f$.

It's worth mentioning that the Δn_s here is determined by the product of the Δn of LC host and its weight ratio. This is different from previous model developed for BPLC, in which Δn_s is used as a fitting parameter. Thus, only two fitting parameters are used in our model: E_s and e_f , instead of Kerr constant K and e_f in Lorenz's model. But now we don't need to set a limit of the strongest electric field that effectively induces birefringence. Taking the voltage shielding effect into account, the simulation result using our model is plotted as the blue solid line in Fig. 1, which fits well with the measured data. In order to extrapolate the performance of this material with optimized electrode structure, we further calculated VT curves using IPS-2/4 cells with both flat electrodes and 3.5 μ m protruded electrodes as examples. The flat electrode refers to normal ITO electrode, whose height is usually around 40nm. In these two cases, the PI layer was changed into photo-alignment layer to reduce the voltage shielding effect, which has $\epsilon_{AL} = 3.9$ and $d_{AL} = 30$ nm. Now the electric field intensity near electrodes is stronger than IPS-15/15. But for flat electrodes, the electric field penetration depth is shallow so the on-state voltage just drops a little as the red solid line in Fig. 1. As the dead zone area above electrodes is decreased, a higher transmittance ($\sim 64\%$) is achieved. Protrusion electrodes have been commonly used to lower the operation voltage of blue phase LCDs. A typical protrusion height is from 2 μ m to 4 μ m [23–25]. And the simulation result is shown as pink solid line in Fig. 1. The cell now achieves a peak transmittance of $\sim 66\%$ at $V = 22V_{rms}$, much better than IPS-15/15 because dead zone area decreases and average electric field intensity as well as penetration depth increase. Notice that the refraction of light inside the

cell has not been taken into account yet, which could result in a higher transmittance in small dimension cell like IPS-2/4 [26].

The fitting results are: $E_s = 7.32\text{V}/\mu\text{m}$ and $e_f/k = 0.78\text{ V}^{-1}$, where k is the average of the splay (k_{11}) and bend (k_{33}) elastic constants. The fitting results are quite reasonable compared to previous studies. When the same LC host was employed in polymer-stabilized BPLC cells, its Kerr constant is $\sim 6\text{-}8\text{ nm}/\text{V}^2$. The Kerr constant of our HTN cell is found to be $5.22\text{ nm}/\text{V}^2$ from following equation:

$$K = \frac{\Delta n_s}{\lambda E_s^2}. \quad (6)$$

According to Gerber's model [27]:

$$K \sim \frac{\Delta n \cdot \Delta \varepsilon \cdot p^2}{k}, \quad (7)$$

the Kerr constant is proportional to p^2 . This model is widely used in analyzing the electro-optical effects of short-pitch blue phase system. Notice that the Bragg reflection wavelength for BPLC can be expressed as $\lambda = 2na / \sqrt{h^2 + k^2 + l^2}$, where a and n denote lattice constant and average refractive index of BPLC, and h , k and l are the Miller indices of a crystal plane. Usually we cure BPLC at BP-I, where the lattice constant $a = p$ and the crystal plane corresponding to the longest reflection peak is (110). Therefore, the longest Bragg reflection wavelength of BPLC is $\lambda_0 = \sqrt{2}np$. We usually adjust the Bragg reflection wavelength at $\sim 350\text{nm}$ for polymer-stabilized BPLC, so the pitch length is comparable to this HTN cell. However, they have different structure assembling, with double twist cylinder lattice structure is formed in BPLC while only one dimensional chiral nematic LC structure exists in our HTN sample, so Kerr effect may not be as strong as in BPLC. This is the reason that our fitted Kerr constant is similar to that obtained from BPLC cell, but a little smaller. The fitted e_f/k value of our material is larger than that of 5CB [28], but still smaller than some bimesogen materials which have larger flexoelectric coefficient [29]. As analyzed above, the induced birefringence is mainly contributed by the Kerr effect. Because the large $\Delta \varepsilon$ material causes a strong Kerr effect, which responds intensely when the voltage is relatively low, while the flexoelectro-optic effect will grow rapidly at higher voltage.

3.2 Temperature dependent response

To investigate the temperature effect, we measured the VT curves of our HTN cell under different temperatures (0 - 60°C) and their on-state voltages are plotted in Fig. 2. As we can see, the on-state voltage first decreases and then increases as temperature elevates. At room temperature, the on-state voltage is around 102V. If we divide this voltage by the 15- μm electrode gap, then the corresponding electric field is $E \sim 6.8\text{V}/\mu\text{m}$. Please note this is only a rough estimate because the electric field in an IPS cell is not uniform. This value is by far the lowest ever been reported in USH devices [17, 18]. A simple reason is that our LC host has a large $\Delta \varepsilon$ and high Δn , leading to a large Kerr constant. As shown in Fig. 2, the optimal operation temperature of our device occurs at around room temperature so that the device would be stable in a wide temperature range when used around room temperature. One reason is that the Kerr constant has a peak value at the optimal operation temperature [15].

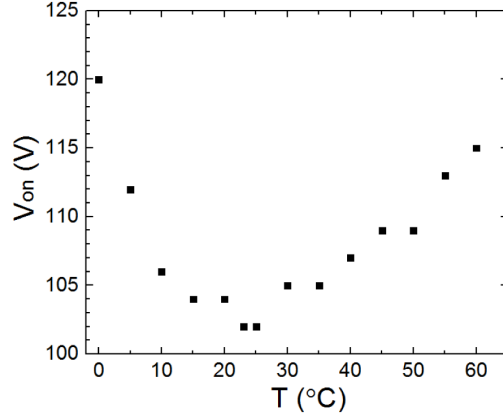


Fig. 2. Measured on-state voltage of the HTN sample at different temperatures.

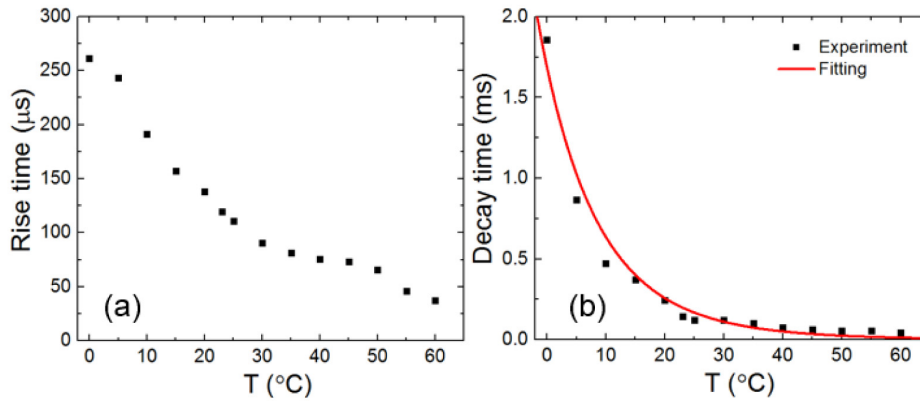


Fig. 3. Temperature dependent rise (a) and decay (b) time. Dots are experimental data and line represents fitting using Eq. (8) with $B = 6 \times 10^{-13}$ ms.

In addition to the VT characteristics, we also investigated the temperature effect on the dynamic responses of our HTN cell. The corresponding on-state voltage at each measured temperature was applied to the cell and then removed. The transient transmittance change was recorded by a digital oscilloscope. The measured rise and decay times (10-90% transmittance change) were plotted in Fig. 3(a) and 3(b), respectively. The rise time is shorter than $300\mu\text{s}$ in the entire measured temperature range. If the HTN cell is operated above room temperature, the rise time is even faster than $100\mu\text{s}$. The primary reason for faster rise time at high temperatures is because of the reduced viscosity. At low temperature, although the on-state voltage also increases (Fig. 2), the viscosity increases more dramatically, resulting in a slower rise time. On the other hand, the decay time keeps increasing as the temperature decreases, and reaches over 1ms at 0°C . Since the rise process is electric field-driven while the decay process is spontaneous relaxation, we focus on the latter to illustrate the physical properties of the material. We use the following equation [9] to fit the experimental data:

$$\tau = B \frac{E_a / k_B T}{(1 - T / T_c)^\beta}, \quad (8)$$

where B is a proportionality constant, E_a is the activation energy of molecular rotation, and k_B is the Boltzmann constant. Here we assume the pitch length does not change significantly with temperature [30] due to the stabilization by the polymer networks. For many nematic LC materials studied, β is around 0.19-0.26 [31, 32]. Although Eq. (8) involves 3 unknowns, β of

the host material is measured as 0.210. Two fitting parameters can be obtained as $E_a = 667\text{meV}$ and $B = 6 \times 10^{-13}\text{ms}$. The large E_a results from the high viscosity of the large $\Delta\epsilon$ nematic host and chiral dopant. Amazingly, the decay time remains very fast even at low temperature ($<1\text{ms}$ at 5°C and $<2\text{ms}$ at 0°C). It is faster than pure Kerr and flexoelectric effects at low temperature, making it very attractive for photonic applications. We also measured the frequency-dependent response time in the $60\text{Hz}\sim 1\text{kHz}$ region, and it did not vary too much.

3.3 Dynamic response

To evaluate the individual contribution of Kerr and flexoelectric effects, we studied the dynamic relaxation processes of the polymer-stabilized HTN cell. The black solid dots in Fig. 4 show the measured transient decay process of the cell. We first fitted the experimental data with following single exponential relaxation equation [33]:

$$\varphi(t) = A_0 e^{-t/t_0}, \quad (9)$$

where t_0 is the decay time constant. The fitting results are plotted by the blue dashed lines in Fig. 4. As we can see, the single exponential equation does not fit the experimental results very well, indicating that there are indeed more than one process involved in the relaxation. Therefore, we extend Eq. (9) to include double relaxation processes, as shown below:

$$\varphi(t) = A e^{-t/t_1} + B e^{-t/t_2}. \quad (10)$$

Here, t_1 and t_2 are the decay time constants; while A and B represent the individual phase retardations from flexoelectric effect and Kerr effect, respectively. Since transmittance is proportional to $\sin^2(\varphi(t)/2)$, the fitting results (red solid curve) in Fig. 4 shows that Eq. (10) well describes the decay process. From fittings, t_1 is found to be $27.2\mu\text{s}$, well correlates with the response time of the flexoelectric effect [17]. However, t_2 is much longer ($205.7\mu\text{s}$), and this number well matches with the response time of the Kerr effect [33]. Nevertheless, both time constants are much faster than the response time of nematic LCs. So we can draw a conclusion that the flexoelectric effect significantly exhibits its own characteristic in response time.

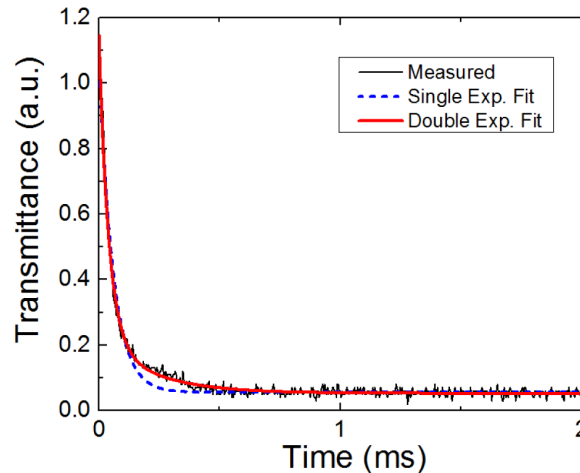


Fig. 4. Measured transient decay process (black solid line) and fittings with single exponential decay (blue dashed curve) and double exponential decay (red solid line).

4. Conclusion

In conclusion, we fabricated a USH cell with a large $\Delta\epsilon$ polymer-stabilized HTN material and studied the coupled Kerr and flexoelectro-optic effects. The sample exhibits low operation voltage while keeping fast response time in a relatively wide temperature range (0~60°C). Also, the optimal operation voltage is around room temperature, which is a big advantage for making practical electro-optic devices. And this HTN material is cured at room temperature, which does not need precise temperature control, thus simplifies the fabrication process. Our proposed model considering both extended Kerr model and shielding effect of alignment layers agrees well with experimental data. Good agreement between experiment and simulation is also obtained in temperature-dependent dynamic response of the HTN cell. All the fittings explain well about the underlying physics, which provides useful guidelines for future material and device optimizations. We should optimize material to find a balance between Kerr effect and flexoelectric effect according to different applications.

Acknowledgment

The UCF group is indebted to Minggang Hu for useful discussion and AFOSR for financial support under contract No. FA9550-14-1-0279.